Supporting Information

Modeling spatial variations of black carbon particles in an urban highway-buildings environment

Zheming Tong[a], Yan Wang[a], Molini Patel[b], Patrick Kinney[b], Steven Chrillrud[c] and K. Max Zhang[a]

[a]Sibley School of Mechanical and Aerospace Engineering, Cornell University, Ithaca, NY 14853, USA
[b]Department of Environmental Health Sciences, Mailman School of Public Health, Columbia University, 60 Haven Avenue, New York, NY 10032, USA
[c]Lamont-Doherty Earth Observatory, Columbia University, Palisades, NY 10964, USA

S1. Overview of CTAG Model

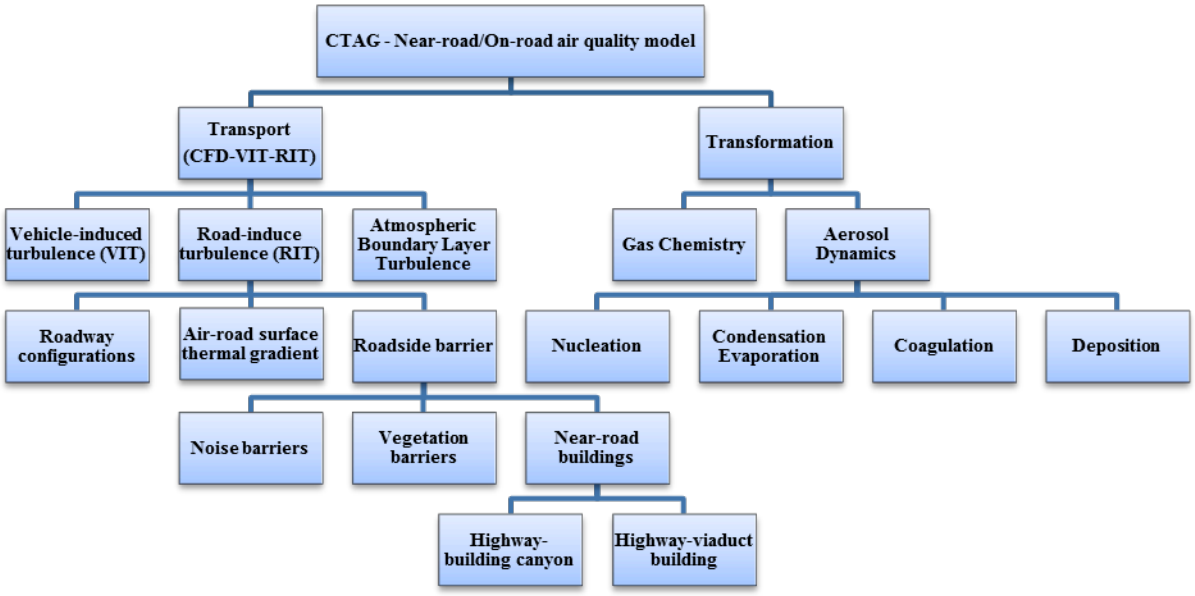

Figure S1: CTAG Model summary

Comprehensive Turbulent Aerosol and Gas Chemistry (CTAG) model is a CFD-based turbulent reacting flow model designed to simulate the transport and transformation of multiple

air pollutants on and near roadways. Figure S1 describes the structure and the components in CTAG. More details about the model can be found in the related publications.[1-3]

We adopted a steady standard k-epsilon turbulence model in our study of the highway-building environment as it has been shown more computationally stable and less intensive for isothermal flow.[4] All the fluid properties such as density, viscosity, surface temperature, and specific heat are assumed to be constant throughout the simulations in order to save computational cost. In terms of solution methods, the SIMPLE pressure-based segregated algorithm is employed which uses a relationship between velocity and pressure corrections to implement conservation and to achieve the pressure field.[5] The gradients for constructing values of a scalar at the cell faces and velocity derivative are computed by Least Squares Cell-Based method. The accuracy of the least-squares gradient method is superior to the cell-based gradient, and comparable to the node-based gradient for irregular meshes[6] while costing less computationally. For computing momentum, turbulent kinetic energy, turbulent dissipation rate, species transport, and energy, the second order accuracy is desired for this study. Thereby, the second-order upwind scheme is employed. The higher order accuracy is accomplished at cell surfaces by a Taylor series expansion of the cell-centered solution about the cell centroid. The first-order scheme is needed to start with and then switched to the second-order scheme after the first-order converges, because in general, the first-order discretization generates better convergences than higher order schemes. Hence, in terms of convergence, it is helpful to first obtain guess values from the first-order scheme, and then set them as initial guess values for the second-order calculation. The residual sum for each of the conserved variables is computed and stored in the end of each iteration. Residuals approach zero as the solution converges. The criterion for judging convergence is listed in Table S1:

Table S1: Convergence Criterion

	Continuity	x,y,z-velocity	Energy	k	Epsilon	BC
Residual	5×10^{-4}	5×10^{-4}	10^{-6}	10^{-3}	10^{-3}	5×10^{-4}

S2. Modeling domain and Discretizing Technique

The dimension of the domain is appropriate according to actual highway geometry and roadside buildings, computational consideration, and the location of the sampling sites. Structures that are located 400m further from the sampling site are not considered as they only have minor or no impact on the transport of BC based on our sensitivity study. The envelope of buildings and highway are geometrically simplified and created in *Solidworks2010* (Figure 1). In addition, the height of the domain is sufficient to ensure that the upper boundary of the computational domain does not impact any pollutant dispersion. The terrain of the domain was captured by *Google Earth* and imported to *Solidworks2010* to ensure that the relative distances among highways and buildings are accurate. The modeling domain is discretized into computational cells with *ANSYS Meshing*, and discretized governing equations are solved inside each cell. The total number of cells is about 2 million. Both a greater number of 5 million and a smaller number of 0.5 million were tested, and the number of cells used captures both the saving in computational cost and the accuracy of pollutant dispersion. A tetrahedron mesh was employed along with a growth rate toward the boundary of air domain. The growth rate was imposed on all discretized cells with a value of 1.03. This greatly saves the computation time as it is not necessary to discretize the whole domain with the same size. For instance, the height of the domain is 150m. However, the highest structure in the model is 45m. Thus, the cells elevated higher than that are not as significant as the elements below 45m. The minimum cell size is 0.5m

on the emission zone of highway. The maximum cell size is about 10m at the bounds of the air domain.

S3: Boundary Conditions

Since the basic logarithmic velocity profile is not applicable for non-adiabatic conditions and the atmosphere is not adiabatic most of the time, we employ the *Monin-Obukhov similarity* for the non-adiabatic cases,[7] in which the wind velocity profile is described by a power law function:

$$\bar{u}_x(z) = \bar{u}_x(h_r)(\frac{z}{h_r})^p \qquad (1)$$

where h_r is the reference height of the measurements; p is determined from the atmospheric stability and surface roughness; z is the position normal to the ground. p is determined from the atmospheric stability and surface roughness; z is the position normal to the ground. The method to estimate p as a function of surface roughness z_0 and *Monin-Obukhov length L* is provided by Huang.[8] *Monin-Obukhov length L* is the height at the point where the turbulence caused by buoyancy equals that caused by mechanical forces. It represents the stability of the atmospheric surface layer. The degree of stability or instability of the atmosphere generally influences the vertical movement of air, which plays a significant role in pollutant transport in urban areas. (See Supporting Information (Table S2) for values of L for different stability conditions.) The power law index p is calculated as a function of L and z_0 as described in Huang.[8] For instance, when the atmosphere is unstable, the values of p vary from 0.05 to 0.2 for

smooth surfaces. However, in very stable conditions, the values of p could range from 0.35 to unity depending on the surface roughness. The values of p ranges from 0.60 to 0.72 based on the surface roughness and stability length calculated.

The inlet k-epsilon turbulence parameters are defined by the following equations:[9]

$$k = \frac{u'^2}{0.3}(1 - \frac{z}{\delta})^2 \qquad (2)$$

$$\epsilon = \frac{C_\mu^{\frac{3}{4}} k^{\frac{3}{2}}}{K\, z} \qquad (3)$$

where u'^2 is the variance of wind speed; δ is the estimated atmospheric boundary layer thickness; z is the position normal to the ground; and K is the Karman constant. The ambient wind and turbulence profiles are written into UDFs in *FLUENT*.

At the outlet of the modeling domain, diffusion fluxes for all flow variables in the direction normal to the exit plane are assumed to be zero. Outflow velocity and pressure are consistent with fully developed flow assumption. The top of the domain is set as a symmetry boundary, where there is zero flux for all quantities. A standard wall function that includes the momentum, energy, species transport, and turbulence equations near the wall is employed for the highway and building surfaces in the domain.[10] The ground surface is set as "wall" as well but with a surface roughness length of 2 m.

S4. Comparison of Turbulence Models

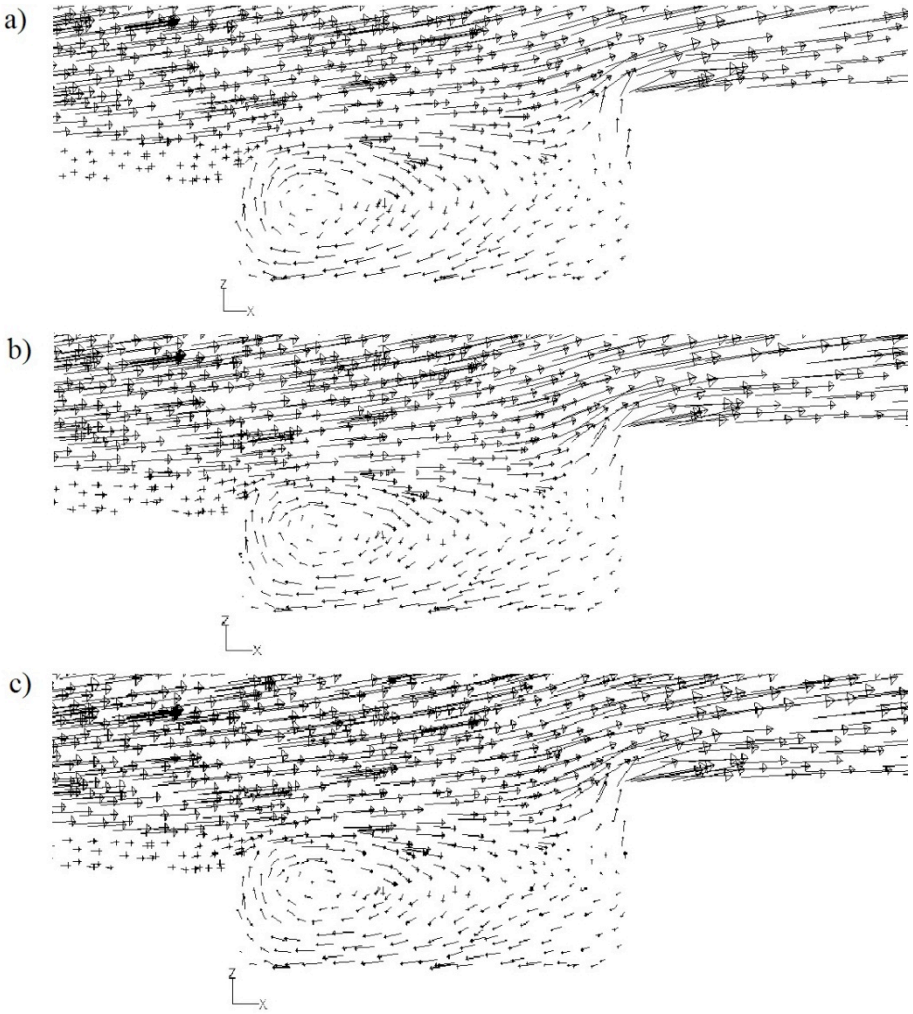

Figure S2: Comparison of simulated flow fields by vectors generated by different turbulent models, a) RNG k-epsilon, b) Standard k-epsilon, c) Realizable k-epsilon

Figure S2 compares the flow field simulations inside the *highway-building canyon* generated by RNG k-epsilon, standard k-epsilon, and realizable k-epsilon turbulence models. The results are similar.

S5. Wind Direction Coordinate Map

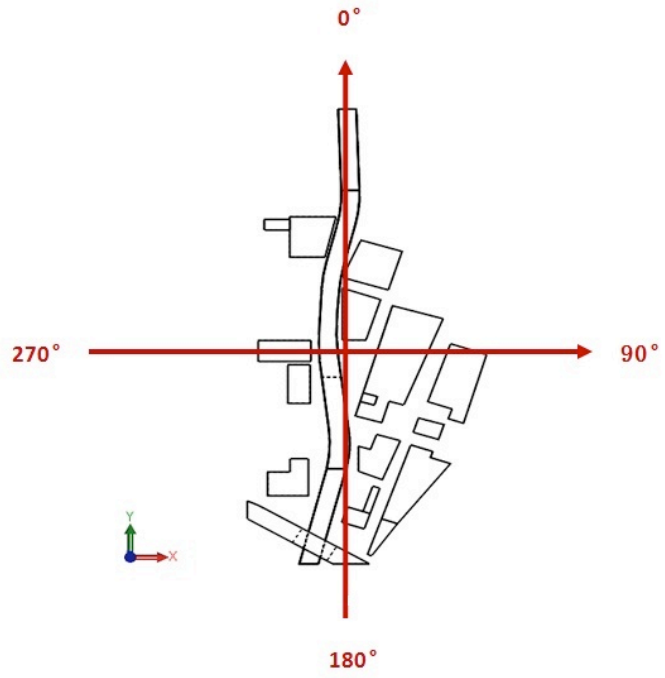

Figure S3: Wind direction Coordinate Map

Figure S3 shows the coordinate of wind direction. We simulated the wind direction from 0 degree to 180 degree due the fact that the measurement point was located on the east side of highway. We only consider the cases where wind is blowing from highway to the measurement point at U2.

S6. Atmospheric Stability

Monin-Obukhov length L represents the stability of the atmospheric surface layer. The degree of stability or instability of the atmosphere generally influences the vertical movement of air, which acts a significant role in pollutant transport in urban areas. In Table S2, typical values of *L* for different stability conditions area given.[11]

Table S2: Stability Condition as a function of *Monin-Obukhov length L*

L	***Stability Condition***
$L<-10^{-5}$	Neutral
$-10^{-5}\leq L\leq -100$	Unstable
$-100\leq L\leq 0$	Very Stable
$0\leq L\leq 100$	Very Stable
$100\leq L\leq 10^{5}$	Stable
$L\geq 10^{5}$	Neutral

S7: Street Canyon

In the street canyon, the concentration is low at the top and high near the bottom in the case where there is a rotating vortex. Most pollutant accumulates at the base of the leeward wall, and becomes less contaminated as the height increases.[12] The presence of the vortex also leads to higher concentrations of pollutants on the leeward wall than the windward.[13] Hoydysha and coworkers studied the flow kinematics in step-up canyons, where one side of the canyon is higher than the other.[14] They concluded that the concentration is a factor of two or greater on the leeward wall compared with windward for step-up and even conditions. In addition, for step-up case, concentrations are typically a factor of two lower in contrast to the step-down and equal cases.

S8. Flow Fields of Different Aspect Ratios

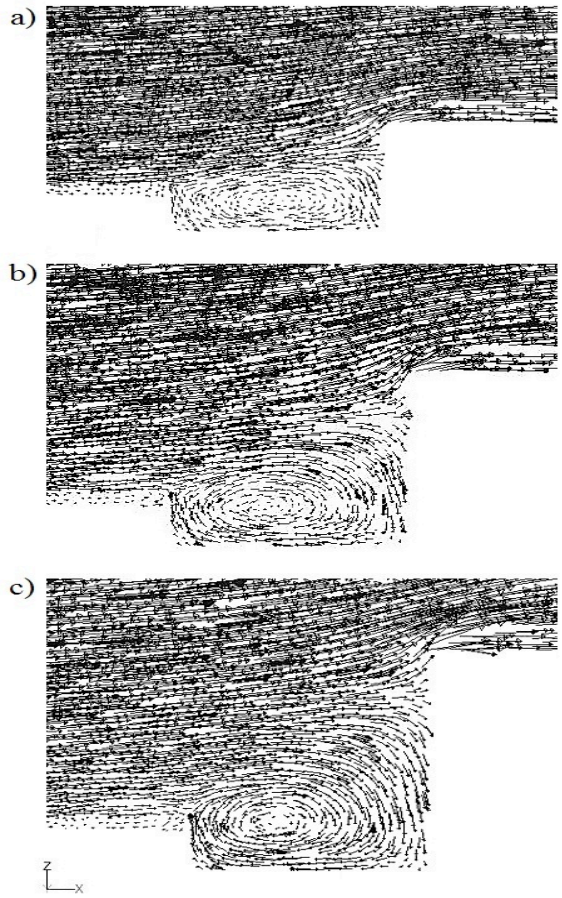

Figure S4: a) 25m (H/W=0.58) b) 35m (H/W=0.75) c) 45m (H/W=0.92)

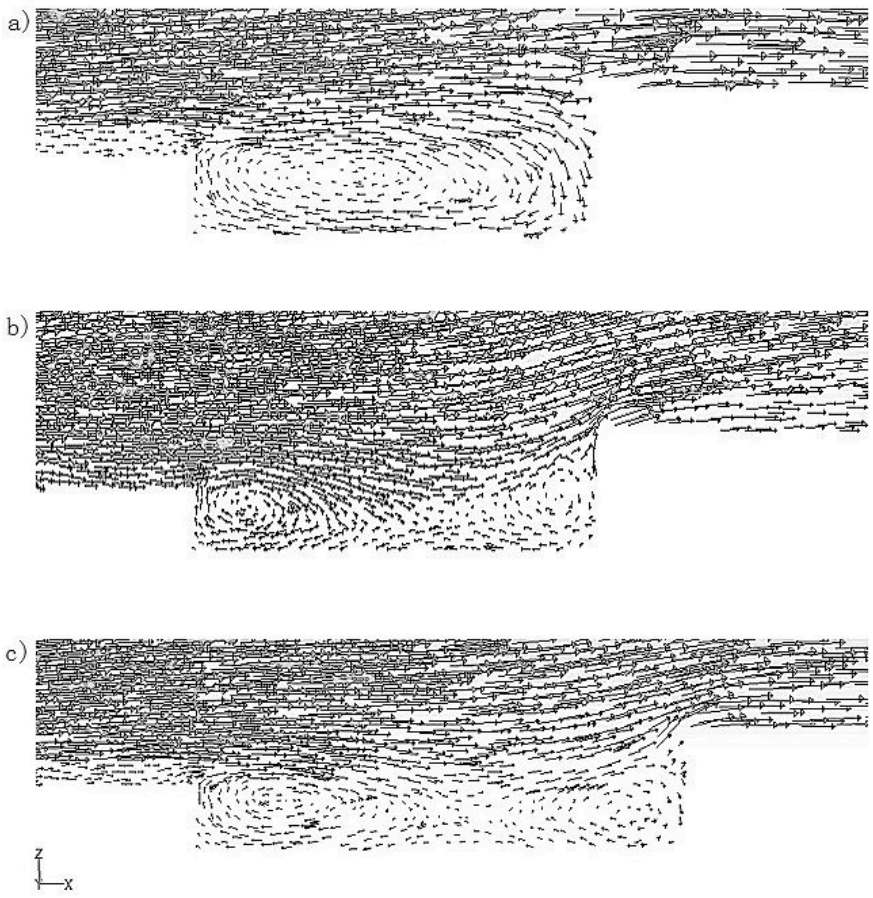

Figure S5: a) 10m (H/W=0.31) b) 20m (H/W=0.25) c) 30m (H/W=0.21)

Figure S4 and Figure S5 depict the flow fields shown by vectors of different aspect ratios inside the *highway-building canyon*. Figure S4 shows the variation of flow fields in the canyon as the height of U2 increases to 25m, 35m, and 45m, corresponding to the BC vertical profiles in Figure 5a. The strength of the circulation vortex amplifies when the height of the windward wall increases (i.e., the front gate of U2). Figure S5 shows the change of flow fields in the canyon as U2 is moved away from highway by 10m, 20m, and 30m, corresponding the BC vertical profiles in Figure 5b. The flow field transitions from one major eddy to two smaller ones.

S9: Corrected Emission rates

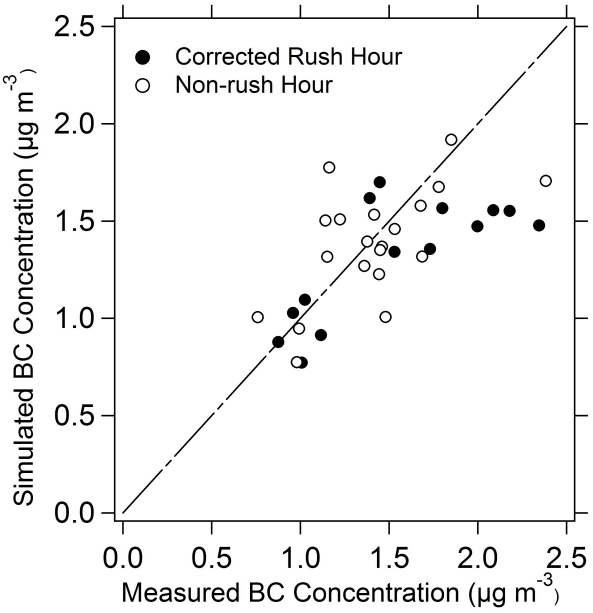

Figure S6: Comparison between measured and predicted BC concentrations with 20% increase of the heavy-duty diesel vehicles in Category II during morning rush hour

The default fraction of heavy-duty diesel vehicles in Category II is 76% in the NYC region.[15] Our best estimate of this fraction is close to 90% during the morning rush hours based on the traffic videos the modeling section is 91% based on the observation on traffic videos during rush hours. As illustrated in Figure S6, increasing BC emission rates during the morning rush hours significantly improves the modeling performance.

Table S2: Wind direction/Speed, Traffic volume, and Emission rates

Wind Direction	Wind Speed (m/s)	Date	Cars	Trucks/Buses	$1/L^a$	Emission factor(kg/m^3-s)
202.5 (SSW)	3.1	3/20/04 8:00 AM	5480	235	-3.39E-03	2.43E-10
	5.7	3/20/04 10:00 AM	6125	330	-4.73E-03	3.32E-10
225(SW)	6.2	3/20/04 11:00AM	7620	220	-5.69E-03	3.32E-10
270 (W)	7.2	3/12/04 7:00AM	7145	705	7.86E-04	6.72E-10
	13.9	3/12/04 8:00AM	7515	830	-1.13E-04	7.86E-10
	18	3/12/04 9:00AM	6435	735	-2.11E-04	6.95E-10
	14.9	3/12/04 10:00AM	5735	770	-1.82E-04	7.21E-10
	4.6	3/15/04 6:00AM	3863	540	1.53E-02	5.05E-10
	6.7	3/15/04 8:00AM	7260	990	-9.52E-04	9.27E-10
	11.3	3/15/04 9:00AM	6435	1245	-6.10E-04	1.14E-09
	9.3	3/15/04 10:00AM	4965	960	-1.59E-03	8.86E-10
	4.1	3/15/04 1:00PM	5295	810	-2.41E-03	7.54E-10
	8.2	3/15/04 3:00PM	6495	630	-2.72E-03	6.01E-10
292.5(WNW)	11.8	3/12/04 12:00PM	5930	825	-8.07E-04	7.72E-10
	10.3	3/12/04 1:00PM	7452	1028	-2.52E-04	9.62E-10
	10.3	3/12/04 2:00PM	5924	572	-2.29E-04	5.46E-10
	10.3	3/12/04 3:00PM	5313	560	-1.52E-04	5.32E-10
	9.3	3/15/04 12:00PM	5370	885	-2.72E-03	8.22E-10
	5.1	3/15/04 4:00PM	5145	510	-2.48E-03	4.86E-10
315(NW)	9.8	3/12/04 11:00AM	5980	805	-6.88E-04	7.54E-10
	10.8	3/12/04 4:00PM	6726	499	-4.62E-04	4.86E-10
	8.7	3/13/04 6:00AM	3735	245	1.12E-03	2.41E-10
	11.3	3/13/04 7:00AM	4925	255	8.04E-04	2.57E-10
	10.3	3/13/04 9:00AM	6575	310	-5.70E-04	3.17E-10
	10.8	3/13/04 1:00PM	7995	280	-2.97E-03	2.99E-10
	8.7	3/22/04 6:00AM	5775	615	1.65E-03	5.83E-10
	11.3	3/22/04 7:00AM	7440	900	8.10E-04	8.48E-10
	10.8	3/22/04 9:00AM	6405	765	-1.47E-03	7.21E-10
	9.8	3/22/04 2:00PM	3810	645	-5.14E-03	5.98E-10
	8.2	3/22/04 3:00PM	3345	510	-3.70E-03	4.75E-10
337.5 (NNW)	8.7	3/13/04 8:00AM	5675	260	-1.13E-04	2.66E-10
	10.3	3/13/04 12:00PM	6575	310	-2.94E-03	2.90E-10
	8.2	3/13/04 4:00PM	7820	155	-1.78E-03	1.86E-10
	6.7	3/22/04 4:00PM	4095	570	-3.10E-03	5.33E-10

[a]:L is *Monin-Obukhov length* .

Table S3:

Statistical Methods	BC without emission correction	BC with emission correction
Mean Normalized Error (MNE)	19.98%	17.33%
Mean Normalized Bias (MNB)	-10.06%	-4.95%
Mean Fraction Error (MFE)	14.23%	12.30%
Mean Fraction Bias (MFB)	-8.25%	-5.35%
R^2	0.39	0.53

Comparison between the performance metrics between the predicted BC concentrations without and with emission correction

7. Reference

(1) Wang, Y. J.; Zhang, K. M. *Environ.Sci.Technol* **2009**, *43*, 7778.

(2) Wang, Y. J.; DenBleyker, A.; McDonald-Buller, E.; Allen, D.; Zhang, K. M. *Atmospheric Environment* **2011**, *45*, 43.

(3) Wang, Y. J.; Zhang, K. M. *Atmospheric Environment* **2011**.

(4) Finlayson, E. U.; Gadgil, A. J.; Thatcher, T. L.; Sextro, R. G. *Indoor Air* **2004**, *14*, 272.

(5) Van Doormaal, J. P.; Raithby, G. D. *Numerical Heat Transfer* **1984**, *7*, 147

(6) Rosenfeld, M.; Marom, G.; Bitan, A. *Boundary-Layer Meteorology* **2010**, *135*, 89.

(7) Monin, A. S.; Obukhov, A. M. *Trans. Geophys. Inst. Akad. Nauk* **1954**, *24*, 163.

(8) Huang, C. H. *Atmospheric Environment (1967)* **1979**, *13*, 453.

(9) Launder, B. E.; Spalding, D. B. *Lectures in Mathematical Models of Turbulence*; Academic Press: London, England, 1972.

(10) Launder, B. E.; Spalding, D. B. *Computer Methods in Applied Mechanics and Engineering* **1974**, 3(2):269.

(11) Seinfeld, J. H.; Pandis, S. N. *Atmospheric Chemisty And Physics: From Air Pollution to Climate Change*; Wiley-Interscience, 2006.

(12) Oke, T. R. *Energy and Buildings* **1988**, *11*, 103.

(13) Nazridoust, K.; Ahmadia, G. *Journal of Wind Engineering and Industrial Aerodynamics* **2006**, *94*, 491.

(14) Hoydysha, W. G.; Dabberdtb, W. F. *Atmospheric Environment* **1988**, *22*, 2677.

(15) *MOBILE 6.2 PM10/PM2.5 EMISSION FACTORS FOR REGIONAL,MESOSCALE,CMAQ,AND MICROSCALE AIR QUALITY ANALYSES, Appendix A -VEHICLE DISTRIBUTIONS BY NYSDOT REGION*, New York State Department of Transportation